Influences of Two-Scale Roughness Parameters on the Ocean Surface Emissivity From Satellite Passive Microwave Measurements

Sang-Moo Lee, *Member, IEEE*, Albin J. Gasiewski, *Fellow, IEEE*, and Byung-Ju Sohn

Abstract—In this study, a method for estimating two-scale roughness influences on the ocean surface emissivity is developed by solving a simplified two-scale ocean emissivity model equation. In this model, scatterings by small-scale roughness are described by the Kirchhoff approximation. For large-scale roughness, the mean local incidence angle (LIA) is introduced to describe slanted surface slope deviation from flat surface. This study focuses on the ocean state under low/moderate wind conditions in order to preclude foam and anisotropic influences within the model. Consequently, a unique pair of two-scale roughness parameters are estimated from the equation using observed ocean emissivities from AMSR2-measured radiances. The results show that the estimated small-scale roughness at 6.925 and 10.65 GHz is linearly correlated with the 10-m height wind speed U_{10}. As the frequency reaches 36.5 GHz, however, the scatters between small-scale roughness and U_{10} are increased, which suggests that the Kirchhoff bistatic scattering function is not fully suitable to describe the small-scale roughness at this frequency. The linear relationships between mean LIA and U_{10} are found with high correlation coefficients. In addition, the estimated mean LIA corresponds well with associated roughness calculated from both observed and modeled ocean wave height spectra. This evidence demonstrates that the proposed large-scale roughness parameterization is physically meaningful and, therefore, the mean LIA has a physical basis in large-scale roughness. In addition, the strong correlations between the roughness parameters and U_{10} demonstrate the possibility to estimate U_{10} from the AMSR2 data using intermediate parameters that are physically based on ocean surface characteristics.

Index Terms—Emissivity, large-scale roughness, microwave, ocean, passive microwave remote sensing, small-scale roughness, wind speed.

I. INTRODUCTION

A FLAT sea surface emits highly polarized microwave radiances which can be theoretically described as a function of incident angle using Fresnel reflection theory with a suitable

Sang-Moo Lee is with the Department of Electrical, Computer, and Energy Engineering, University of Colorado Boulder, Boulder, CO 80309 USA, and also with the National Snow and Ice Data Center, University of Colorado Boulder, Boulder, CO 80309 USA (e-mail: dr.sangmoolee@gmail.com, sang-moo.lee@colorado.edu).

Albin J. Gasiewski is with the Department of Electrical, Computer, and Energy Engineering, University of Colorado Boulder, Boulder, CO 80309 USA.

Byung-Ju Sohn is with the School of Earth and Environmental Sciences, Seoul National University, Seoul 08826, Republic of Korea, and also with the Key Laboratory for Aerosol-Cloud-Precipitation of China Meteorological Administration, School of Atmospheric Physics, Nanjing University of Information and Technology, Nanjing 210044, China.

dielectric constant model. When the sea surface becomes roughened by surface wind stress, the emitted microwave radiances are generally intensified and less polarized [1]. To a first order, the influence of surface roughness on the ocean surface microwave emissivity is largely isotropic and consists of three different types of roughness [2]. One is the large-scale roughness by ocean wave swell that causes surface facets to become tilted, resulting in an average local incidence angle (LIA) that differs slightly from the observation angle [3]. Another is the small-scale roughness by gravity–capillary waves atop the large gravity waves which causes nonspecular scattering of microwaves [4], [5]. The third is sea foam roughness which is primarily produced by the breaking of ocean surface waves and resulting air entrainment. Ocean foam makes the surface generally less reflective in both vertical and horizontal polarizations [6]. The reduction in reflectivity can be expected by dielectric matching of the bulk seawater with the air of comparatively small dielectric constant compared with the seawater [6]. Spatial distributions of gravity–capillary waves and foam are moderately inhomogeneous over the large-scale waves due to boundary layer air turbulence, gravity wave spectral spreading, and differences between large-scale ocean wave propagation and wind direction [1], [7], [8]. The relationship between wind direction and directional spectra for both large-scale and gravity–capillary waves provides the capability to measure wind direction from passive microwave emissivity (or radiance) measurements, but the dominant influence of wind on emissivity under low to moderate wind speeds (<10 m/s or Beaufort 0–5) is through isotropic roughening [1].

Determination of an accurate ocean surface emissivity model is crucial for not only the observation of ocean parameters from passive microwave measurements but also for data assimilation for the numerical weather forecasting. In order to measure the ocean surface wind speeds with an uncertainty of 1.0 m/s, for instance, an accuracy level in the emissivity signal of ~1.0 K is necessary [2]. Numerous studies have shown a clear relationship between ocean surface roughness parameters and local wind stress [4], [6], [9]–[12]. Since wind-roughened sea surface emissivity differs from that of the flat ocean surface, these relationships have been a basis for retrieving sea surface parameters from passive microwave measurements. For example, sea surface wind speed has been obtained from space borne passive microwave measurements based on sea surface emissivity variations by wind-induced surface roughness using both physical and statistical approaches [13], [14]. In sea surface salinity retrieval, surface roughness has been used to correct wind speed influences

on the algorithm itself [15]. Although numerous algorithms are based on the aforementioned theoretical relationships, the model uncertainty in emissivity caused by surface roughness remains higher than desirable for many climate and weather applications. The discrepancy in emissivity variation with respect to wind speed exhibited by several different ocean emissivity models is up to a factor of two [11], [16].

To model the microwave emissivity over the wind-roughened ocean surface, a two-scale approach has been well studied and widely accepted. This nonspecular approach is constructed from a tilt-based geometrical optics emissivity model for large-scale waves with a small-scale emission model for four Stokes' parameters for small-scale waves [5], [8], [10]. However, this model needs too large computational resources to use for practical applications. Therefore, a simplified two-scale ocean surface emissivity model has been developed, based on curve fitting, preserving the accuracy of the more rigorous two-scale model outputs [2], [17]–[19]. This simplified version of the two-scale model is able to produce accurate ocean surface emissivity at microwave frequencies, leading to the successful assimilation of microwave radiances into weather forecast models over the ocean. Since this simplified model is a parametric model whose parameters are fit to the rigorous two-scale model, the two-scale roughness parameters described in this model are difficult to be considered as physical quantities [20]. For instance, in the simplified two-scale model [17]–[19], the Fresnel reflectivities are scaled by the Kirchhoff scattering factor only for coherent waves, after which additional corrections are made in order to account for large-scale roughness effects. This approach misses the correlation between the small- and large-scale influences on the ocean surface emissivity. In other words, coherent bistatic scattering occurs over a flat ocean surface rather than over a large-scale tilted surface. Therefore, it is not physically deemed enough for inversions to estimate small- and large-scale roughness parameters simultaneously from microwave radiances even if it produces accurate forward sea surface emissivity calculations.

By considering the two-scale roughness correlation, a simplified system of equations for microwave ocean surface emissivity calculation was proposed [20] using a physically based parameterization for two-scale roughness. The proposed approach suggested a roughness description whereby the large-scale roughness is expressed as a function of the mean LIA and then bistatic scattering by small-scale roughness occurs using Fresnel theory on the slanted surfaces with orientation determined by mean LIA. The relationship between the two-scale roughness parameters and wind speed needs to be further investigated to evaluate whether this model equation can produce plausible rough surface emission behavior at microwave frequencies. In this study, the simplified two-scale ocean surface emissivity model [20] is used to determine the relationship between small- and large-scale roughness parameters and the surface wind speed based on satellite microwave observations. The simplified equation system proposed by Lee and Sohn [20] when accompanied by a physically based roughness parameterization provides inversion of satellite data for roughness parameters.

The objectives of this study are to develop a satellite-scale algorithm for retrieving small- and large-scale surface roughness parameters assuming a foamless ocean by solving the simplified two-scale ocean surface microwave emissivity equation at microwave frequencies [20] and to evaluate whether the simplified two-scale model can describe plausible two-scale roughness parameters. In Section II, a review of the simplified two-scale microwave ocean surface emissivity model [20] is presented. Section III describes the retrieval method for small- and large-scale roughness parameters from Advanced Microwave Scanning Radiometer 2 (AMSR2) measurements and other data used in this study. Section IV presents the results of ocean surface roughness mapping and comparison between the retrieved roughness parameters and ocean surface wind speed from AMSR2 measurements. Section V shows independent comparison between the AMSR2-estimated two-scale roughness parameters and buoy-measured wind speed. Section VI discusses the algorithm sensitivity to assumptions, and Section VII is a summary and discussion.

II. THEORETICAL BACKGROUNDS FOR SIMPLIFIED TWO-SCALE OCEAN SURFACE EMISSIVITY MODEL

The followings are description of the simplified two-scale ocean surface emissivity model [20], including the components of dielectric constant and small- and large-scale roughness parameters.

A. Fresnel Reflection

A flat sea surface reflection can be theoretically described by the Fresnel reflection theory [27], [28]

$$r_v(\varepsilon, \theta) = \left| \frac{\varepsilon \cos \theta - \sqrt{\varepsilon - \sin^2 \theta}}{\varepsilon \cos \theta + \sqrt{\varepsilon - \sin^2 \theta}} \right|^2 \qquad (1)$$

$$r_h(\varepsilon, \theta) = \left| \frac{\cos \theta - \sqrt{\varepsilon - \sin^2 \theta}}{\cos \theta + \sqrt{\varepsilon - \sin^2 \theta}} \right|^2 \qquad (2)$$

where ε is the dielectric constant of a material, and r_v and r_h are the vertically and horizontally polarized Fresnel reflectivities, respectively. Equations (1) and (2) imply that the specular sea surface emissivities at an observation angle θ with respect to the surface normal can be determined when the dielectric constant of seawater is prescribed. In this study, Meissner and Wentz's dielectric model [24] is adopted because it has been validated with an extensive analysis of special sensor microwave/imager (SSM/I) brightness temperature (T_B) observations at the frequencies of interest in this study. Since the dielectric constant of seawater is calculable from the model [24] with given sea surface temperature T_{SST} and sea surface salinity S values, the specular ocean surface emissivity is calculable from (1) and (2).

B. Isotropic Surface Roughness Effects

The ocean surface emissivity is mainly influenced by isotropic surface roughness which can be divided into two components: 1) large-scale roughness effects and 2) bistatic scattering by small-scale roughness. Each of these effects and

how they are parameterized in the simplified two-scale ocean surface emissivity model are described below.

1) Slant Surface by Large-Scale Roughness: Wind-induced large-scale gravity waves cause deviations of the ocean surface from flatness, resulting in the LIA differing from the mean earth incidence angle (EIA; θ_{EIA}) of the satellite observation. Due to the nonlinearities in (1) and (2) with respect to LIA and the large-scale statistics of LIA, the emission will be in error if only EIA is used as an input for (1) and (2). One way to relate the large-scale roughness to emission is to find a mean LIA for the distribution of ocean surface facets based on an isotropic Gaussian surface height distribution. Therefore, a mean surface emissivity over a statistically tilted sea surface is used along with the Fresnel reflectivity to define a mean LIA [20]

$$e_{p,\mathrm{Fresnel}} = 1 - r_p(\varepsilon, \langle\theta_{\mathrm{LIA}}\rangle) \tag{3}$$

where $e_{p,\mathrm{Fresnel}}$ is the Fresnel surface emissivity over slant ocean surface with the mean LIA $\langle\theta_{\mathrm{LIA}}\rangle$. In such cases, the coherent wave reflectivity is effectively zero relative to the incoherent wave reflectivity, and the mean LIA is assumed to capture the long-wave impact on effective emissivity. This assumption provides a key simplification used in this study. Therefore, the ocean surface emissivity influenced by the large-scale tilted surface can be calculated if $\langle\theta_{\mathrm{LIA}}\rangle$ is provided. Since $\langle\theta_{\mathrm{LIA}}\rangle$ does generally differ from θ_{EIA} by large-scale roughness, $\Delta\theta$ (defined as $\langle\theta_{\mathrm{LIA}}\rangle - \theta_{\mathrm{EIA}}$) can be treated as an index of large-scale roughness [20].

2) Small-Scale Roughness: Small gravity–capillary waves ride on the large gravity waves and are due to the surface tension of water as a restoring force. These gravity–capillary waves cause bistatic surface scattering and absorption which generally serve to change the microwave emission of each tilted facet. The scattering by small-scale roughness [17]–[20] has been described by the coherent part of Kirchhoff's bistatic scattering function K_{coh} [19], [29]–[31]. Therefore, the Fresnel reflectivities are scaled according to

$$r'_p = r_p(\varepsilon, \theta) K_{\mathrm{coh}} \tag{4}$$

where r'_p is the Fresnel reflectivity modified by small-scale roughness at p-polarization, and K_{coh} is defined as follows:

$$K_{\mathrm{coh}} = \exp\left(-4k^2\sigma_{\mathrm{s}}^2\cos^2\theta\right) \tag{5}$$

where σ_{s} is the small-scale surface roughness (i.e., small-scale root mean square (rms) height), and k is the electromagnetic (EM) wavenumber. Since (5) treats coherent scattering only and incoherent scattering becomes stronger with frequency, the assumption inherent in (4) and (5) might not be valid in not accounting for the incoherent reflection. Therefore, incoherent scattering effects should be included in (4). One can rewrite (4) with both coherent and incoherent scattering effects as

$$r'_p = r_p(\varepsilon, \theta) K \tag{6}$$

where K is a small-scale Kirchhoff factor which can be defined as

$$K = K_{\mathrm{coh}} + (1 - K_{\mathrm{coh}})\frac{T_{\mathrm{B}}^{\mathrm{L}}}{T_{\mathrm{B}}^{\downarrow}} \tag{7}$$

where $T_{\mathrm{B}}^{\mathrm{L}}$ is the reflected atmospheric radiance incident from a range of incoherent directions assuming that the surface follows a Lambertian reflection pattern and $T_{\mathrm{B}}^{\downarrow}$ is the downwelling specular atmospheric radiance. In the short ocean wavelength range and for the low to moderate wind speeds considered in this study, the values of σ_{s} are small enough that K_{coh} as defined in (5) is mostly greater than ~0.5. This range suggests that most scattering by small-scale roughness is coherent and largely in the specular direction. A further study of the correlation length l would be valuable to bound the short-scale incoherent scattering of downwelling radiation directions. This directional effect has been modeled using the so-called Ω factor [2], [5], [13] While it is in principle possible to incorporate the effect of the Ω factor into the downwelling distribution of radiance, the impact for this effect is also to some extent modeled by the increase in mean LIA with large-scale surface roughness.

Since the bistatic scattering by small-scale roughness occurs over the statistically tilted surface with mean LIA, the following model relationship is thus obtained by combining (6)–(7) as follows:

$$e'_p = 1 - r_p(\varepsilon, \langle\theta_{\mathrm{LIA}}\rangle)$$
$$\times \left(K_{\mathrm{coh}}(\sigma_{\mathrm{s}}, \langle\theta_{\mathrm{LIA}}\rangle) + (1 - K_{\mathrm{coh}}(\sigma_{\mathrm{s}}, \langle\theta_{\mathrm{LIA}}\rangle))\frac{T_{\mathrm{B}}^{\mathrm{L}}}{T_{\mathrm{B}}^{\downarrow}}\right) \tag{8}$$

where e'_p is the effective ocean surface emissivity over a foamless ocean surface.

C. Ocean Foam and Anisotropic Wind Effects

In addition to the small- and large-scale roughness parameters, there are two additional parameters influencing the ocean surface emissivity: 1) ocean foam and 2) anisotropic wind direction effects. In order to express the foam influence on microwave ocean surface emissivity, the effective ocean surface emissivity e_p is defined by weighting the fraction f_c of the surface with foam coverage and seawater emissivity. For anisotropic wind effects, it is simplistically incorporated by adding an azimuthally dependent emissivity variation into (8) [19]. Therefore, effective ocean surface emissivity in the simplified two-scale model is

$$e_p = f_c e_{p,\mathrm{Foam}} + (1 - f_c)e'_p + \Delta e_\varphi \tag{9}$$

where $e_{p,\mathrm{Foam}}$ is the foam emissivity at p-polarization and Δe_φ is the anisotropic surface roughness influence on the effective ocean surface emissivity.

III. METHOD AND DATA

Since the main objective of this study is to find the relationship between the two-scale surface roughness parameters (i.e., K and $\langle\theta_{\mathrm{LIA}}\rangle$) and wind speed, the effects of foam and wind direction are ignored because those effects are small compared with the two-scale roughness effects under low and moderate wind conditions (<10 m/s or Beaufort 0–5) [1], [2]. According to Wentz [1], there is no correlation between the variation of ocean surface emissivity and wind direction when wind speed is less than 7 m/s. Investigation of wind direction influences on ocean surface brightness by Meissner and Wentz [48]

concluded that there is basically no wind direction signal on the ocean-emanated radiance below 5 m/s. Therefore, it can be assumed that wind direction effects are negligible when wind speed is less than 5–7 m/s. In addition, a sensitivity test shows that the above assumption is valid over wind speeds less than 10 m/s, indicating that influences of ocean foam and wind direction signals on the estimation of two-scale roughness are negligible (Section V). Therefore, (9) can be approximated as (8) by dropping out foam and wind direction effects. One writes (8) for the two linear polarizations as

$$e_v = 1 - r_v(\varepsilon, \langle \theta_{\text{LIA}} \rangle) K(\sigma_s, \langle \theta_{\text{LIA}} \rangle) \tag{10}$$

$$e_h = 1 - r_h(\varepsilon, \langle \theta_{\text{LIA}} \rangle) K(\sigma_s, \langle \theta_{\text{LIA}} \rangle) \tag{11}$$

where the subscripts v and h represent the vertical and horizontal polarizations, respectively. The effective emissivities for the two polarizations on the left-hand side of (10) and (11) can be estimated by computing the ratio between the satellite observed T_Bs after subtracting the atmospheric effects and the sea surface temperature T_{SST} [32], [33]. With known two polarized effective emissivities over the ocean, the remaining unknowns are to be σ_s and $\langle \theta_{\text{LIA}} \rangle$ because ε of seawater can be obtained from the double-Debye relaxation model [24] with the prescribed T_{SST} and S. Since the equation system is now posed (i.e., two equations and two unknowns), a unique pair of K and $\langle \theta_{\text{LIA}} \rangle$ are sequentially estimated using the maximum likelihood (ML) estimator as follows:

$$\left\langle \widehat{\theta}_{\text{LIA}} \right\rangle = \min_{\langle \theta_{\text{LIA}} \rangle} \left[\left(\frac{T_{B_v} - T_{\text{SST}} + T_B^{\uparrow}}{T_{B_h} - T_{\text{SST}} + T_B^{\uparrow}} - f(\langle \theta_{\text{LIA}} \rangle, T_{\text{SST}}) \right)^2 \right] \tag{12}$$

$$\widehat{K} = \frac{1}{2} \sum_{p=v,h} \frac{T_{\text{SST}} e^{-\tau} - T_{B_p} + T_B^{\uparrow}}{r_p \left(\varepsilon, \left\langle \widehat{\theta}_{\text{LIA}} \right\rangle \right) \left(T_{\text{SST}} - T_B^{\downarrow} \right) e^{-\tau}} \tag{13}$$

where $f(\langle \theta_{\text{LIA}} \rangle, T_{\text{SST}}) \triangleq r_v(\varepsilon, \langle \theta_{\text{LIA}} \rangle) / r_h(\varepsilon, \langle \theta_{\text{LIA}} \rangle)$, $T_B^{\uparrow}$ is the upwelling radiance contributions from the atmosphere to the satellite observed radiances, and $e^{-\tau}$ is the atmospheric opacity. The above estimators can be shown to be bivariate sequential ML estimates of the two-scale roughness parameters (the detailed derivation of these ML estimators is provided in Appendix A). In this process, the sea surface reflectivity is assumed to be isotropic. The dielectric constant ε of seawater is obtained from the double-Debye relaxation model [24] with the prescribed T_{SST} and S. Unique pairwise estimates of Kirchhoff factor K and large-scale mean surface tilt angle $\langle \theta_{\text{LIA}} \rangle$ under low to moderate wind using T_{SST} and S products as inputs are obtained. Evaluation of the sensitivity of these estimates to uncertainties in input parameters is addressed in Section V.

In this study, the Satellite Data Simulation Unit (SDSU)-version 2.1 [34] was used to calculate the atmospheric influences on the AMSR2-measured T_Bs with inputs of atmospheric profiles from the European Center for Medium-Range Weather Forecast Reanalysis (ERA)-Interim [35] dataset. In this model, the oxygen absorption is modeled according to Staelin [49] and the water vapor absorption codes are based on Ulaby *et al.* [50]. The cloud liquid water extinction in SDSU is based on the Rayleigh approximation assuming the

nonprecipitating atmosphere. However, this study assumes that the target scene is clear sky. For this study, daily resampled T_Bs at 6.9, 10.7, 18.7, and 36.5 GHz and T_{SST} products were used to estimate $\langle \theta_{\text{LIA}} \rangle$ and K over the global ocean surface. AMSR2 T_B and T_{SST} data on a $0.25° \times 0.25°$ grid were obtained from Japan Aerospace Exploration Agency (JAXA) through their G-portal website (http://gportal.jaxa.jp). Due to the strong influence of the water vapor absorption line at the 22.235 GHz, the AMSR2 23.8-GHz measurements were not considered in this study. In order to estimate the dielectric constant of seawater, T_{SST} estimates from AMSR2 and climatological S from the World Ocean Atlas [36] were used. In order to exclude the influences on precipitating and/or heavy clouds on the algorithm, the pixels for which columnar cloud liquid water from the ERA-Interim dataset is greater than 0.3 mm were excluded [12]. Wind speed products obtained from both AMSR2 measurements (http://gportal.jaxa.jp/) and ocean surface wind speed from buoy measurements (https://www.pmel.noaa.gov/tao/drupal/disdel/) were used to analyze the retrieved ocean surface roughness parameters with wind speeds over the global ocean surface. AMSR2 wind speed product has bias and rms difference of -0.22 and 1.09 m/s (respectively) against buoy-measured wind speed. In this study, any correction has not done for AMSR2 wind speeds. The detailed explanations for buoy-measured wind speed are provided in Section V.

IV. RESULTS

Based on the developed ML estimator with AMSR2-measured T_Bs, this section provides geographical distributions of the calculated two-scale roughness parameters over the global ocean and compared them with AMSR2 wind speeds. Fig. 1 shows the geographical mappings of the estimated K factor at 6.925, 10.65, 18.7, and 36.5 GHz over the global ocean for April 1, 2015. It is noted that K over ocean decreases with increasing frequency, consistent with the physics of the Kirchhoff approximation in that bistatic scattering is enhanced as frequency increases [4]. Under the condition of wind speed less than 10 m/s, the averaged K values over the global ocean are 0.987, 0.975, 0.957, and 0.941 for 6.925, 10.65, 18.7, and 36.5 GHz, respectively. This suggests that small-scale roughness induces specular reflection reductions of $\sim1.3\%$ at 6.925 GHz and $\sim5.9\%$ at 36.5 GHz under low to moderate wind conditions. Spatial distributions of Ks correspond closely to the wind speed distribution at 10 m above the sea surface (U_{10}) from AMSR2 measurements (Fig. 2), which might be expected because the K factor and U_{10} wind speeds are both obtained from the AMSR2 data. However, we expect that small-scale roughness is related to enhanced gravity–capillary waves induced by wind forcing. Fig. 3 shows 2-D histograms between K at four different frequencies and U_{10}. As expected, Ks are near unity in the case of a calm sea surface (i.e., $U_{10} < 1$ m/s or Beaufort 0), which is consistent with the theoretical expectation because gravity–capillary waves do not exist without near-surface wind stress. For a wind speed lower than 3 m/s, the estimated Ks are between 0.98 and 1.0, regardless of frequency, indicating that the small-scale roughness at best changes the Fresnel reflectivity by no more
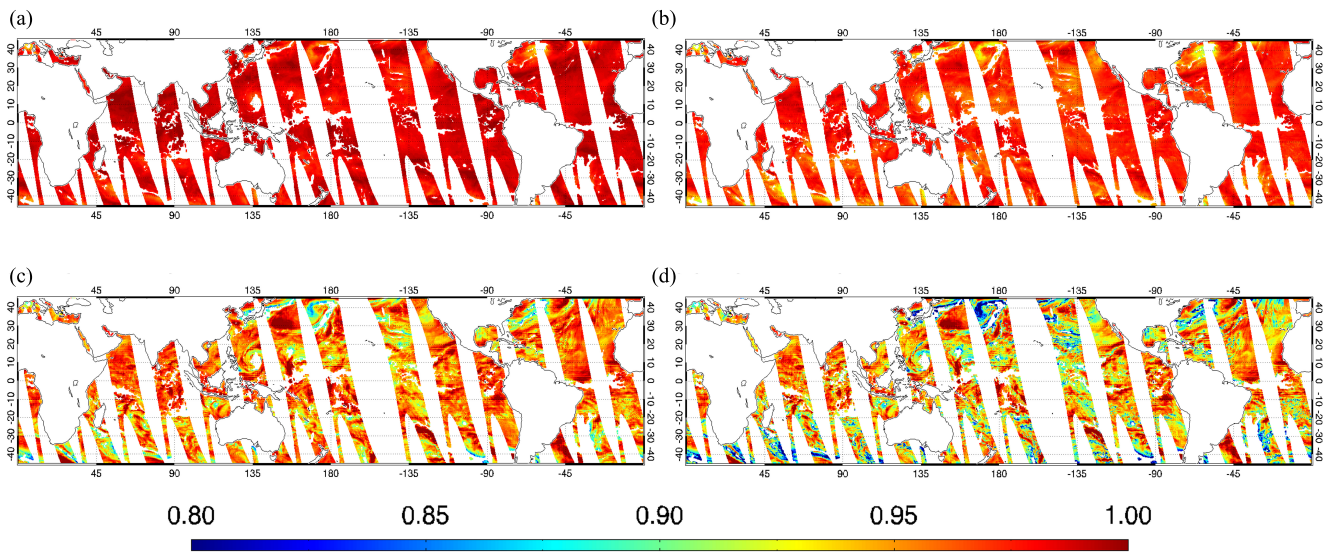
Fig. 1. Geographical distributions of the AMSR2-estimated Kirchhoff scattering factor (K) at AMSR2 frequencies of (a) 6.925 GHz, (b) 10.65 GHz, (c) 18.7 GHz, and (d) 36.5 GHz for April 1, 2015.
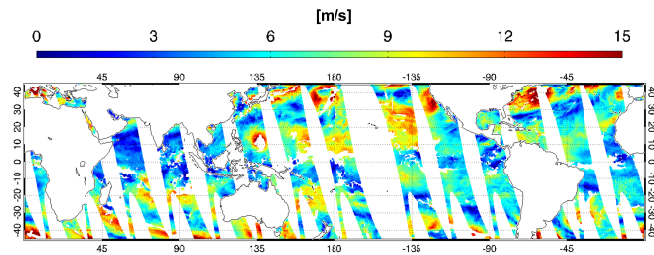

Fig. 2. Geographical distributions of wind speed at 10 m above the sea surface from AMSR2 measurements for April 1, 2015.

than 2%. For frequencies of 6.925 and 10.65 GHz, there is a strong linear relationship between K and U_{10} with correlation coefficients above 0.9. As frequency increases, more scatter is observed between these two variables. This scattered pattern especially for higher frequencies is possibly due to the atmospheric noises. In addition, there is a limitation of the simplified two-scale ocean surface emissivity model which is not able to explicitly model the statistical wave height spectrum dependence of scatterings by small-scale roughness. Since emissivity changes by small-scale roughness are dependent on not only LIA but also wind-induced wave height spectrum, simple parameterizations such as (7) fall short of predicting the small-scale roughness. Nonetheless, we study this model as a means of improving the simplistic parametrization within the simplified two-scale model.

Spatial distributions of the mean LIA $\langle\theta_{LIA}\rangle$ at the four different frequencies are shown in Fig. 4. The geographical distributions of $\langle\theta_{LIA}\rangle$ are similar to the distributions of K and U_{10}, and $\langle\theta_{LIA}\rangle$ becomes larger as frequency increases. Calculations of $\langle\theta_{LIA}\rangle$ for Gaussian surfaces with Gaussian correlation functions indeed show that $\langle\theta_{LIA}\rangle$ increases monotonically with ocean slope variance when incoherent reflectivity dominates. This can be demonstrated by comparing both the theoretical and predicted $\Delta\theta$ and ocean slope variances calculated from a semiempirical ocean wave height spectrum, which will be discussed henceforth. At frequencies between
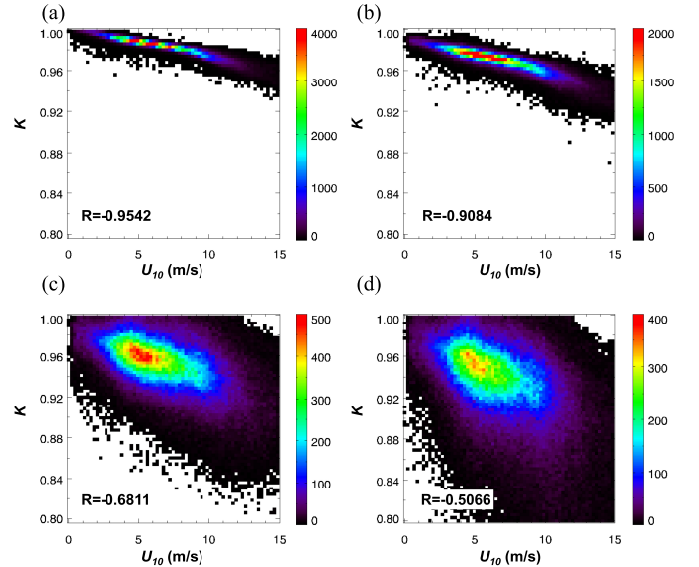

Fig. 3. Two-dimensional histogram between (*y*-axis) the estimated Kirchhoff scattering factor at (a) 6.925 GHz, (b) 10.65 GHz, (c) 18.7 GHz, and (d) 36.5 GHz and (*x*-axis) wind speed at 10 m above the sea surface from AMSR2 measurements. Bin sizes are 0.25 and 0.002 for the *x*- and *y*-axes, respectively. The comparison period is April 1–7, 2015. Correlation coefficients are provided in the diagram.

6.925 and 18.7 GHz, values of $\langle\theta_{LIA}\rangle$ are near 55° which is θ_{EIA} of AMSR2 measurements, showing that the large-scale roughness influences on effective Fresnel emissivity are small at these frequencies. As the frequency reaches 36.5 GHz, significantly larger $\langle\theta_{LIA}\rangle$ is observed. The mean value of $\langle\theta_{LIA}\rangle$ at 36.5 GHz under wind speeds less than 10 m/s is 58.1° which implies a 12.7% difference in vertical (worst case) Fresnel emissivity between $\langle\theta_{LIA}\rangle$ and θ_{EIA} of AMSR2. Contrary to the K distribution at 36.5 GHz, a relatively smooth global spatial distribution of $\langle\theta_{LIA}\rangle$ at 36.5 GHz is obtained and it is noted that the spatial distribution of ocean surface wind speed is highly correlated with the distribution of $\langle\theta_{LIA}\rangle$ at 36.5 GHz. A direct comparison between $\Delta\theta$ and
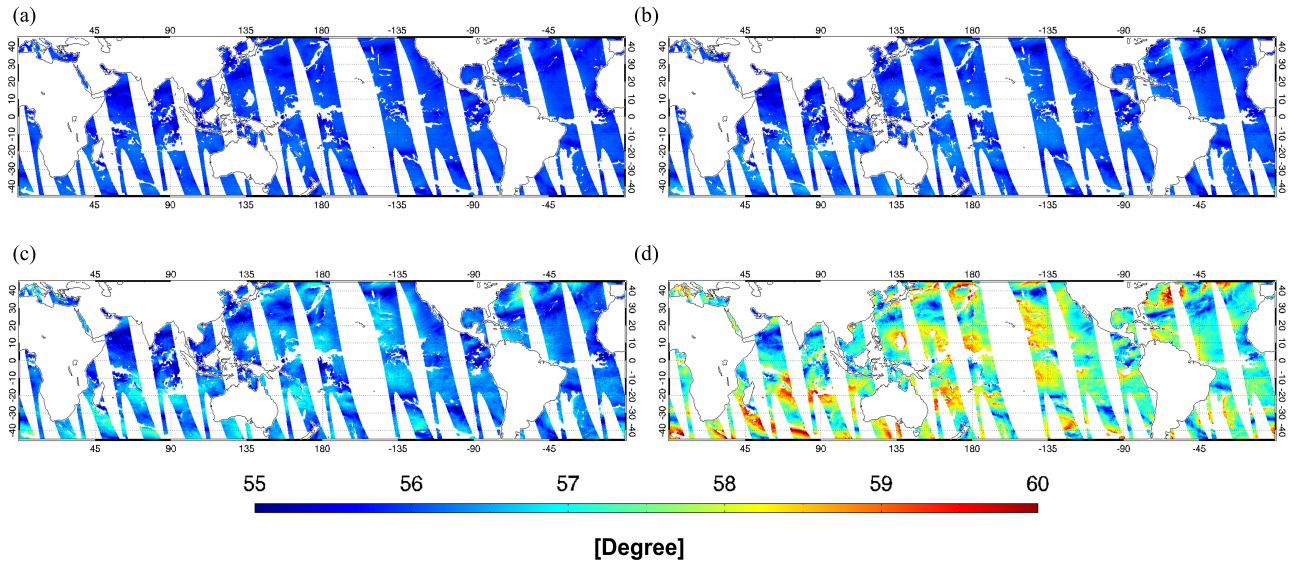
Fig. 4. Geographical distributions of estimated $\langle \theta_{LIA} \rangle$ using AMSR2 data at frequencies of (a) 6.925 GHz, (b) 10.65 GHz, (c) 18.7 GHz, and (d) 36.5 GHz for April 1, 2015.
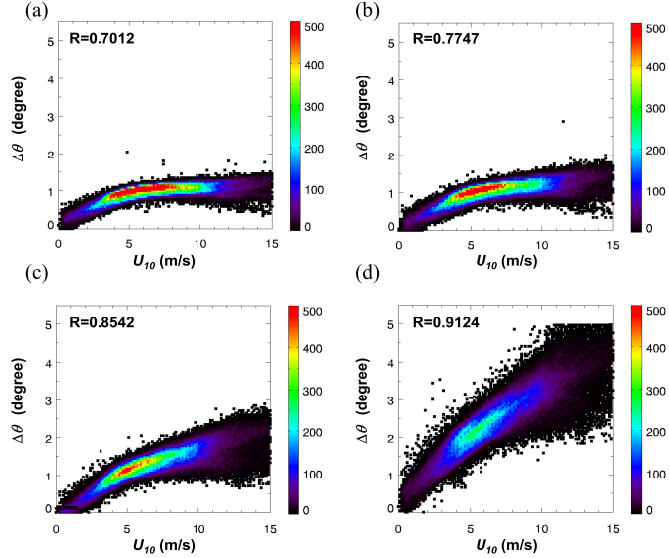

Fig. 5. Two-dimensional histograms between (ordinate) estimated $\Delta\theta$ at (a) 6.925 GHz, (b) 10.65 GHz, (c) 18.7 GHz, and (d) 36.5 GHz and (abscissa) wind speed at 10 m above the sea surface from AMSR2 measurements. Bin sizes are 0.1 and 0.25 for the x- and y-axes, respectively. The comparison period is April 1–7, 2015. Correlation coefficients Rs are shown.

U_{10} is made and illustrated in Fig. 5. Contrary to small-scale roughness, large-scale roughness behavior with respect to U_{10} is approximately logarithmic. It is noted that the relationship between $\Delta\theta$ and U_{10} tends to be closer as frequency increases, which is opposite to the relationship between K and U_{10}. Particularly for frequencies of 6.925 and 10.65 GHz, $\Delta\theta$ tends to saturate when the wind speed is higher than $\sim$9 m/s, converging to approximately 1°. Similar phenomena were observed in the curvature spectrum of ocean waves, for which the rms curvature of a wind-driven ocean surface tends to saturate as wind speeds become stronger [7], [37]. In contrast, the increasing trend in $\Delta\theta$ saturation at higher frequencies indicates a larger short wave surface roughness scale division. However, at both low and high frequencies, $\partial(\Delta\theta)/\partial U_{10}$ tends

to decrease with U_{10}, indicating that $\Delta\theta$ eventually saturates at limiting values of U_{10} that are frequency dependent.

We note that from the generalized Phillips–Kitaigorodskii equilibrium range parameter [37]–[39], the ocean surface curvature spectrum for the long-wave portion of the ocean wave spectrum is enhanced as wave age decreases. From this study, the surface tilt by large-scale ocean waves is closely related to the ocean wavenumber relative to the EM wavenumber. From these observations, it can be expected that the estimated $\langle\theta_{LIA}\rangle$ is correlated with the slope variance $\langle s^2 \rangle$ of (specifically) large-scale ocean waves. Furthermore, the mean LIA can also be calculated from a given $\langle s^2 \rangle$ under the assumption that ocean surface follows an isotropic Gaussian height distribution with Gaussian correlation function. Therefore, it is of interest to compare the estimated $\langle\theta_{LIA}\rangle$ from AMSR2 T_Bs and the modeled slope variance $\langle s^2 \rangle$ [and the corresponding model-based $\langle\theta_{LIA}\rangle$ (hereafter referred to as $\langle\theta'_{LIA}\rangle$)] from a semiempirical ocean surface wave height distribution. If $\langle\theta_{LIA}\rangle$ is correlated with $\langle s^2 \rangle$ and $\langle\theta'_{LIA}\rangle$, then this is strong evidence that the suggested large-scale roughness parameterization of $\langle\theta_{LIA}\rangle$ is valid. In order to calculate $\langle s^2 \rangle$ and $\langle\theta'_{LIA}\rangle$, the wave height model of Durden and Vesecky (hereafter referred to as the DV model) was used [40]. A detailed discussion of the DV model and how it is used to estimate $\langle s^2 \rangle$ and $\langle\theta'_{LIA}\rangle$ are provided in Appendix B. Considering the long-wave ocean spectrum only, the integration interval used to obtain $\langle s^2 \rangle$ with respect to ocean wavenumber k_0 is restricted from 0 to $k_l = k/10$ where k is the EM wavenumber [5] and k_l is the upper cutoff ocean integration wavenumber.

Fig. 6(a) illustrates the resulting relationship between $\Delta\theta$ (i.e., $\Delta\theta = \langle\theta_{LIA}\rangle - \theta_{EIA}$) and $\langle s^2 \rangle$, and Fig. 6(b) shows the relationship between $\Delta\theta$ and $\Delta\theta'$ (i.e., $\Delta\theta' = \langle\theta'_{LIA}\rangle - \theta_{EIA}$) under low and moderate wind conditions. Both relationships reveal an approximately linear relationship between $\Delta\theta$ and $\langle s^2 \rangle$, and between $\Delta\theta$ and $\Delta\theta'$. Although $\langle\theta_{LIA}\rangle$ represents the mean ocean slope reflection angle from the flat specular ocean surface while $\langle s^2 \rangle$ indicates the variance of ocean surface
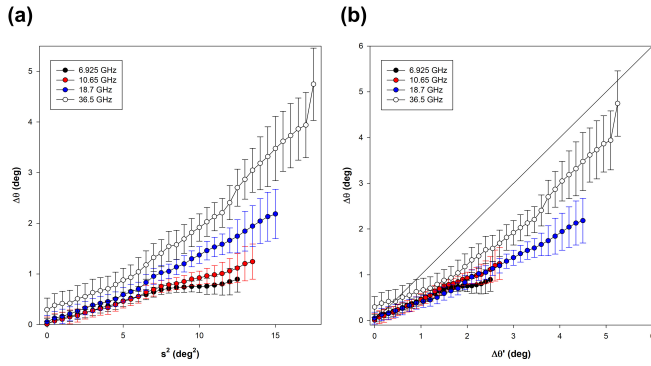
Fig. 6. (a) Relationships between $\Delta\theta$ and $\langle s^2 \rangle$ and (b) $\Delta\theta$ and $\Delta\theta'$ at four different frequencies of (black dots) 6.925 GHz, (red dots) 10.65 GHz, (blue dots) 18.7 GHz, and (open circles) 36.5 GHz.

slope at a certain mean slope, they are both linearly related. As the surface becomes rough, the relationship between them seems to be parabolic. Nevertheless, the obtained relationship between $\Delta\theta$ and $\Delta\theta'$ with high correlation coefficient (>0.95) demonstrates that the proposed large-scale roughness parameterization in the suggested simplified two-scale model is able to plausibly describe scatterings by large-scale roughness.

Although $\Delta\theta$ is always smaller than $\Delta\theta'$, this is understandable because the magnitude of the $\Delta\theta'$ calculation from the DV model is largely dependent upon the selection of k_l which is selected as $k/10$ without strong physical basis. Since k_l is considered to be the EM wavenumber scaled by an arbitrary factor, a more accurate one-to-one correspondence between $\Delta\theta$ and $\Delta\theta'$ should be able to be obtained once a more reliable k_l criterion is prescribed to calculate $\Delta\theta'$.

V. COMPARISON WITH BUOY-MEASURED WIND SPEED

Buoy-measured wind speed data at 3.5–4.0 m above the sea surface can also be used as an independent comparison between the estimated two-scale roughness and wind speed. Selected buoy data are a combination of measurements from: 1) the Tropical Atmosphere Ocean (TAO) buoys supported by National Oceanic and Atmospheric Administration (NOAA) and the Japan Agency for Marine-Earth Science and Technology (JAMSTEC) and 2) the Prediction and Research Moored Array in the Tropical Atlantic (PIRATA) buoys supported by Meteo-France, Center for Weather Forecasting and Climate Studies (CWFC), and NOAA. The period of buoy measurements used is April and May for both 2014 and 2015. These buoy-measured ocean surface wind speed data were obtained from the Pacific Marine Environmental Laboratory website (https://www.pmel.noaa.gov/tao/drupal/disdel/). For spatiotemporal collocation, the AMSR2 data are paired with the closest buoy data only if the center point of a given AMSR2 footprint is located within 25 km of the buoy position. Otherwise, temporal collocation occurs by averaging AMSR2 and buoy data on a daily basis. AMSR2-buoy pairs are discarded if the corresponding columnar cloud liquid water from ERA-Interim database is greater than 0.3 mm.

Comparisons of two-scale AMSR2 roughness parameters and buoy wind speeds are presented in Fig. 7. In these results, we correlate buoy-based wind speeds at points with AMSR2 data representing averages over a larger area
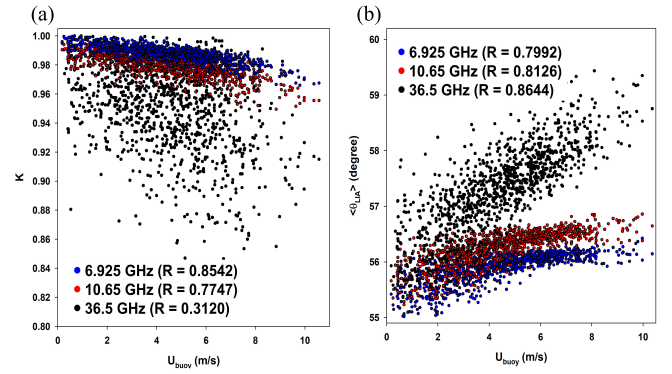

Fig. 7. Scatterplots between (ordinate) (a) estimate Kirchhoff factor K and (b) mean LIA $\langle\theta_{LIA}\rangle$ and (abscissa) buoy-measured wind speed U_{buoy} for frequencies of (blue dots) 6.925 GHz, (red dots) 10.65 GHz, and (black dots) 36.5 GHz. Blue, red, and black points represent the linear fits for 6.925, 10.65, and 36.5 GHz, respectively.
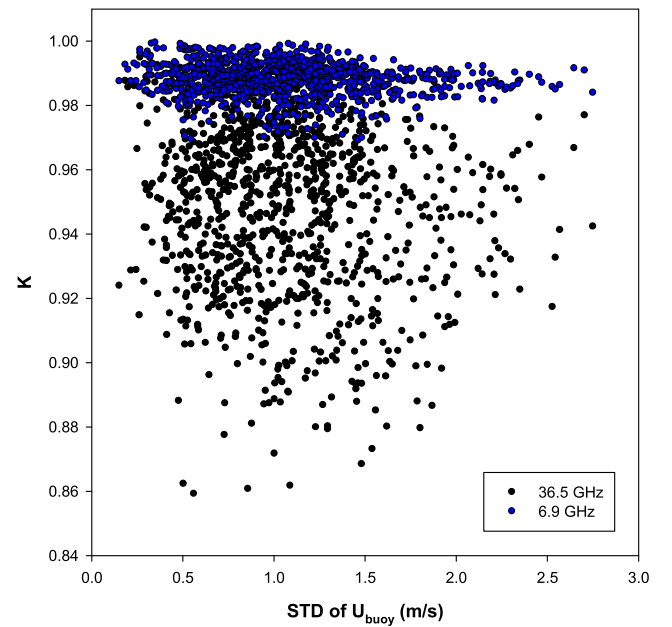

Fig. 8. Scatterplots between (ordinate) the estimate Kirchhoff factor K and (abscissa) buoy-measured standard deviation of wind speed U_{buoy} on a daily basis for frequencies of (blue dots) 6.925 GHz and (black dots) 36.5 GHz.

within 25 km of the buoy location. Thus, local wind fluctuations measured by the buoy are not well represented in the larger satellite-observed pixel because wind gusts are dominated by local pressure fluctuations. Nevertheless, the comparison results indicate that both of the two-scale roughness parameters from the AMSR2 measurements are mostly well correlated with buoy-measured wind speed. At lower frequencies, small-scale roughness is linearly correlated with wind speed, with correlation coefficients near 0.85. However, K at 36.5 GHz and diurnally averaged buoy-measured wind speed are weakly related but not well correlated. Due to K being a factor that presumably responds rapidly to wind stress, it is hypothesized that at least as close a relationship exists between K and the level of local wind fluctuations (i.e., gustiness) within an AMSR2 footprint. We explore this hypothesis by analyzing K versus local buoy wind speed standard deviation as a measure of gustiness (Fig. 8). While the buoy wind

TABLE I

SENSITIVITY OF KIRCHHOFF FACTOR WITH RESPECT TO SEA
SURFACE TEMPERATURE (T_{SST}) IN °C, SEA SURFACE SALINITY
(S) IN PPT, TROPOSPHERIC COLUMN WATER VAPOR (V) IN MM,
AND ATMOSPHERIC MEAN TEMPERATURE (T_{ATM}) IN KELVIN
AT FIXED 55° INCIDENCE ANGLE

Freq.	$\partial K/\partial T_{SST}$	$\partial K/\partial S$	$\partial K/\partial V$	$\partial K/\partial T_{ATM}$
6.9 GHz	0.0022	-0.0001	0.0001	0.0001
10.7 GHz	0.0020	0.0000	0.0002	0.0001
18.7 GHz	0.0015	0.0000	0.0003	0.0002
36.5 GHz	0.0005	0.0000	0.0003	0.0003

TABLE II

SENSITIVITY OF LOCAL MEAN INCIDENCE ANGLE WITH RESPECT TO SEA
SURFACE TEMPERATURE (T_{SST}) IN °C, SEA SURFACE SALINITY (S) IN
PPT, TROPOSPHERIC COLUMN WATER VAPOR (V) IN MM, AND
ATMOSPHERIC MEAN TEMPERATURE (T_{ATM})
IN KELVIN WITH $K = 1$

Freq.	$\partial\theta_{LIA}/\partial T_{SST}$	$\partial\theta_{LIA}/\partial S$	$\partial\theta_{LIA}/\partial V$	$\partial\theta_{LIA}/\partial T_{ATM}$
6.9 GHz	-0.1355	0.0034	-0.0245	-0.0104
10.7 GHz	-0.1267	0.0012	-0.0447	-0.0108
18.7 GHz	-0.1010	0.0003	-0.0599	-0.0133
36.5 GHz	-0.0565	0.0001	-0.0692	-0.0171

speed standard deviation was calculated over a 24-h period, there is nonetheless a weak relationship between K and wind fluctuation level at both 6.9 and 36.5 GHz, validating the association of K with short-scale roughness.

For $\langle\theta_{LIA}\rangle$, we obtain nearly the same results using the buoy wind data as were found in the comparison between $\langle\theta_{LIA}\rangle$ and AMSR2 U_{10}. Overall, however, the AMSR-estimated K at 36.5 GHz is only weakly correlated with both averaged buoy wind speed and standard deviation. We thus recognize that K as defined in (7), while an improvement over the definition used in (5), is still not fully suitable to describe the small-scale scattering at the higher microwave frequencies. The small-perturbation method can be used for an alternative method to describe scatterings by small-scale roughness [5], [45], [46], although it needs greater computational cost.

VI. ALGORITHM SENSITIVITY

The algorithm developed for retrieving two-scale roughness parameters from AMSR2-measured polarized T_Bs uses T_{SST}, S, atmospheric temperature, and humidity profiles as inputs. Therefore, it is necessary to examine possible propagated errors due to the uncertainties of these inputs. In order to assess the algorithm sensitivity, we introduce a differential form of K and $\langle\theta_{LIA}\rangle$ with respect to the environmental parameters. Tables I and II show how uncertainties in the environmental parameters are propagated into the estimates of the small- and large-scale roughness parameters, respectively. Nominal values of T_{SST} of 20 °C, S of 35 ppt, and clear sky total columnar water vapor V, and layer-averaged temperature T_{ATM} at a latitude of 10.25 °N and longitude of 160 °E for May 1, 2015 from ERA-Interim are used to calculate the sensitivity of the roughness parameters to T_{SST}, S, V, and T_{ATM}. While error

propagations of surface properties to roughness estimations tend to decrease with increasing frequency, opposite trends are noted in the case of atmospheric quantities. The influences of uncertainties in S, V, and T_{ATM} on K estimates are negligible as evidenced in Table I. For instance, the induced uncertainty level in K due to uncertain S, V, and T_{ATM} is on the order of 10^{-4} to 10^{-5}. However, 1 °C uncertainty in T_{SST} brings about up to 0.5% error in K which corresponds to a T_B error of 0.95 K at 6.925 GHz. Similarly, T_{SST} uncertainties appear to be a major potential error source in $\langle\theta_{LIA}\rangle$ retrievals. These uncertainties are because the accuracy of T_{SST} is directly connected with the accuracy of e_p estimates. It is notable that $\langle\theta_{LIA}\rangle$ error due to the uncertainty of V is comparable with that of SST at 36.5 GHz.

In addition, atmospheric columnar liquid water (hereafter referred to as L) can affect the accuracy of K and $\langle\theta_{LIA}\rangle$ estimations. According to Meissner and Wentz [2] and [48], an error in L of 0.1 mm induces an error in the 37-GHz horizontally polarized brightness temperature of 0.9 K. Since L from atmospheric reanalysis data is very uncertain, an algorithm sensitivity test regarding L is required although this study discarded the scene where L is greater than 0.03 mm. In order to assess L uncertainty influences on the developed algorithm, we use the Rayleigh approximation to estimate absorption by L (the detailed formulation is provided in [2]). In this study, we allow 0.03-mm errors in L to estimate the error propagation due to uncertain L into the algorithm. The result shows that the error induced by L uncertainty is up to 0.5% error in K and 0.7% error in $\langle\theta_{LIA}\rangle$, which is comparable with the expected error due to uncertain T_{SST}. In order to circumvent the possible error associated with uncertain V and L, one can potentially consider a linear combination of $2T_{Bv}-T_{Bh}$ rather than the single polarization for AMSR2 frequencies [48].

Since the influences of sea foam and wind direction on the ocean surface emissivity are assumed to be negligible, the possible error induced by the assumption is worth investigated. To do so, the two-scale roughness parameter estimates from (10) and (11) are compared with those from (9) with the aids of the sea foam coverage model from Monahan and O'Muircheartaigh [6] and the sea foam emissivity model suggested by Stogryn [41]. Differences between these two-scale roughness estimates with and without foam effects are illustrated in Fig. 9. For both two-scale roughness parameters, the differences in with and without foam effects are negligible when U_{10} is less than 10 m/s. At a wind speed of ∼10 m/s, the difference between K with and without foam effects is at largest 0.3%. For the large-scale roughness, a ∼0.15° difference in $\langle\theta_{LIA}\rangle$ at 10 m/s is found, which corresponds to an emissivity error of at most 0.5% at 6.9 GHz. Thus, neglecting foam influences at wind speeds less than 10 m/s is an acceptable assumption. It is noted that the differences in two-scale roughness parameters are exponentially growing with wind speed in this range, indicating that the foam assumption becomes invalid at high wind regions beyond ∼10 m/s.

Since wind direction influences are much smaller than the foam influences, it is expected that the retrieval error due to wind direction uncertainty is much smaller than that due to neglect of foam. Nevertheless, we perform the same test
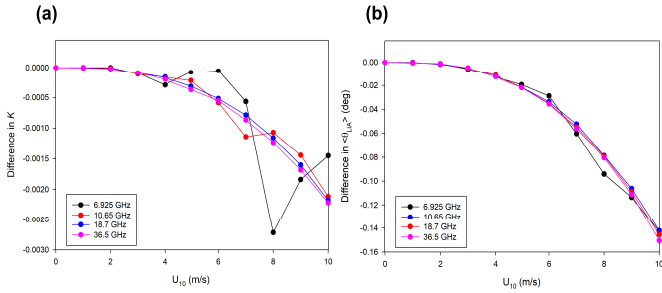
Fig. 9. Differences between roughness parameters K and $\langle\theta_{\text{LIA}}\rangle$ estimated with and without foam influence for (a) K and (b) $\langle\theta_{\text{LIA}}\rangle$.

for wind direction impact by adopting the emissivity versus wind direction parameterization as found in [1]. The wind direction-induced error is on the order of 10^{-7} in K at wind speed of 10 m/s, indicating that error propagation by anisotropic ocean surface behavior is negligible.

In addition to input parameters and assumptions discussed above, the sensor random noise [i.e., noise equivalent differential temperature (NEDT)] can induce an error in K and $\langle\theta_{\text{LIA}}\rangle$ estimations. For AMSR2, the maximum expected NEDTs at 6.925, 10.65, 18.7, and 36.5 GHz are 0.34, 0.7, 0.7, and 0.7 K, respectively [51], [52]. In order to assess the influences of sensor noise on the developed algorithm, the differences in K and $\langle\theta_{\text{LIA}}\rangle$ between AMSR-measured T_{B} with noise and without noise are calculated. The calculation results show that the NEDT causes errors in K and $\langle\theta_{\text{LIA}}\rangle$ estimation at best 0.25%. Furthermore, it is noted that the AMSR2 receivers have rather large nonlinearities, which can cause calibration errors. These errors can also be propagated into K and $\langle\theta_{\text{LIA}}\rangle$ estimations.

VII. Summary and Conclusion

In this study, the parameters of a two-scale roughness model of ocean emissivity at microwave frequencies (here, 6.9, 10.65, 18.7, and 36.5 GHz) at low to moderate wind speeds are estimated over the global ocean surface. In this retrieval, the simplified two-scale ocean surface emissivity equations are used for calculating the two isotropic roughness parameters of $\langle\theta_{\text{LIA}}\rangle$ and K from AMSR2-estimated effective ocean surface emissivities. The model employs the Kirchhoff bistatic scattering function (i.e., K factor) to describe small-scale roughness effects. For large-scale roughness, $\langle\theta_{\text{LIA}}\rangle$ is introduced to describe slanted surface slope deviation from the mean flat surface due to large-scale gravity waves. In doing so, it is assumed that the influences of foam and anisotropic roughness parameters on the microwave ocean surface emissivity are negligible under low to moderate wind conditions. Sensitivity tests show that these assumptions are valid under these conditions. Since the developed ML estimator needs two linearly polarized T_{B} fields, the polarized radiances measured by dual-polarization capable passive microwave sensors such as AMSR2, SSM/I, and WindSat can be used to estimate K and $\langle\theta_{\text{LIA}}\rangle$. In this study, AMSR2-measured brightness temperatures were used as a case in point. For the use of the developed algorithm for higher wind speed than 10 m/s, it is noted that the foam and wind direction influences on e_p are necessarily included.

The spatial distributions of the estimated two-scale roughness parameters over the global ocean from AMSR2 measurements show that both K and $\langle\theta_{\text{LIA}}\rangle$ are strongly correlated with U_{10}. For 6.925 and 10.65 GHz, K is linearly related to U_{10} with correlation coefficients above 0.9. As frequency reaches 18.7 and 36.5 GHz, however, the scatter between K and U_{10} is increased. This evidence suggests that the Kirchhoff bistatic scattering function is not fully suitable to describe the scattering by small-scale roughness at these frequencies.

The relationship between $\langle\theta_{\text{LIA}}\rangle$ and U_{10} becomes more deterministic as frequency increases. Following this evidence, we suggest that the incidence angle variations by large gravity waves play a significant role in determining the ocean surface reflectivity compared with bistatic scattering by small gravity–capillary waves. Indeed, Kunkee and Gasiewski [7] showed that a geometric optics model can produce plausible anisotropic ocean surface emissivity behavior over 10–92 GHz even if bistatic scattering by small-scale roughness is not considered. It is further noted that $\langle\theta_{\text{LIA}}\rangle$ tends to saturate when wind speed increases. Related phenomena are observed in the curvature spectrum of the ocean wave spectral distribution, for which the rms curvature of a wind-driven ocean surface tends to saturate as wind speed increases. In addition, it is found that the estimated $\langle\theta_{\text{LIA}}\rangle$ is highly correlated with the mean slope variance $\langle s^2\rangle$ and long-wave mean angle of incidence $\langle\theta'_{\text{LIA}}\rangle$ of ocean waves calculated from the DV model. This evidence demonstrates that the proposed large-scale roughness parameterization is physically meaningful and, therefore, that $\langle\theta_{\text{LIA}}\rangle$ has a physical basis in large-scale roughness.

It can further be conjectured that the small-scale roughness is related to gust variability in local wind and $\langle\theta_{\text{LIA}}\rangle$ bears information on long-wave ocean fetch and swell. Future investigation into distinguishing wind gust and ocean fetch effects can be done by correlating the estimated K and $\langle\theta_{\text{LIA}}\rangle$ with parameters describing these conditions.

The model equation suggested in this study can be tested whether this equation can improve the forward emissivity calculation based on the simplified two-scale ocean surface emissivity model such as fast microwave emissivity model (FASTEM). It may be possible because e_V and e_H from rigorous two-scale model and/or satellite measurements can be converted into K and $\langle\theta_{\text{LIA}}\rangle$. Therefore, similar to the FASTEM fitting of small- and large-scale roughness parameters with known wide ranges of wind parameters and satellite geometric angles (i.e., satellite zenith and azimuth angles), the estimated K and $\langle\theta_{\text{LIA}}\rangle$ can be regressed to the wind stress over the ocean for forward model calculation purpose. In doing so, the sensitivity test of the proposed model equation with other ocean wave parameters such as wave height spectrum, inverse wave age, and angular spreading effects should be accompanied.

In addition, the strong correlations between the two-scale roughness parameters and U_{10} demonstrate the possibility to estimate ocean surface wind speed from the AMSR2 data using intermediate parameters that are physically based on ocean surface characteristics. We provide here a possible retrieval algorithm for U_{10} based on ML estimation using the sum of squares χ^2 between measured and modeled two-scale

surface roughness, i.e.

$$
\chi^2 = \sum_v \left[\frac{\left(\widehat{K} - K^M(U_{10}) \right)_v^2}{\text{Var}\left[\left(\widehat{K} - K^M(U_{10}) \right)_v \right]} + \frac{\left(\langle \widehat{\theta}_{\text{LIA}} \rangle - \langle \theta_{\text{LIA}} \rangle^M (U_{10}) \right)_v^2}{\text{Var}\left[\left(\langle \widehat{\theta}_{\text{LIA}} \rangle - \langle \theta_{\text{LIA}} \rangle^M (U_{10}) \right)_v \right]} \right]
\tag{14}
$$

where K^M and $\langle \theta_{\text{LIA}} \rangle^M$ are statistical and/or physical models relating K and $\langle \theta_{\text{LIA}} \rangle$ to the wind speed U_{10}. These models can be developed by analyzing the relationship between the estimated two-scale roughness parameters and ocean surface wind speed, fetch, and variability irrespective of any radiative transfer model. Since the differences between measured and modeled two-scale roughness parameters are divided by the expected variances between them in the ML estimator, a precalculation of these expected error variances would be necessary.

APPENDIX A
ESTIMATOR FOR SMALL- AND LARGE-SCALE ROUGHNESS PARAMETERS

The T_Bs measured by AMSR2 consist of surface emission and upwelling/downwelling atmospheric components modeled as

$$
T_{B_v} = e_v T_{\text{SST}} e^{-\tau} + T_B^\uparrow + (1 - e_v) T_B^\downarrow e^{-\tau} + n_v
\tag{15}
$$

$$
T_{B_h} = e_h T_{\text{SST}} e^{-\tau} + T_B^\uparrow + (1 - e_h) T_B^\downarrow e^{-\tau} + n_h
\tag{16}
$$

where $T_B^\uparrow$ and $T_B^\downarrow$ are the upwelling and downwelling atmospheric T_B, respectively. It is noted that $T_B^\downarrow$ is a function of $\langle \theta_{\text{LIA}} \rangle$, $e^{-\tau}$ is the atmospheric opacity, and n_p is the noises at p-polarization associated with the AMSR2 instrument. In this study, we assume that the noises are uncorrelated and follow Gaussian distribution. In this case, the noises can be neglected because the expected value of noises can be treated as zero. As discussed in Section VI, a random error such as NEDT of the sensor can propagate to the developed algorithm itself. However, the influences of AMSR2 NEDTs on the developed algorithm are found to be small. Therefore, the noises n_v and n_h in (15) and (16) can be neglected as

$$
\widehat{e}_v = \frac{T_{B_v} - T_B^\uparrow - T_B^\downarrow e^{-\tau}}{\left(T_{\text{SST}} - T_B^\downarrow \right) e^{-\tau}}
\tag{17}
$$

$$
\widehat{e}_h = \frac{T_{B_h} - T_B^\uparrow - T_B^\downarrow e^{-\tau}}{\left(T_{\text{SST}} - T_B^\downarrow \right) e^{-\tau}}
\tag{18}
$$

where T_{SST} is the sea surface temperature. In this study, T_{SST} is obtained AMSR2 measurements but can also be obtained from buoy measurements or global ocean models.

By computing the ratio of (10) and (11), K factor can be eliminated, upon which $\langle \theta_{\text{LIA}} \rangle$ can be estimated by substituting (15) and (16) into the computed ratio as

$$
\langle \widehat{\theta}_{\text{LIA}} \rangle = \min_{\langle \theta_{\text{LIA}} \rangle} \left[\left(\frac{1 - \widehat{e}_v}{1 - \widehat{e}_h} - f\left(\langle \theta_{\text{LIA}} \rangle, \widehat{T}_{\text{SST}} \right) \right)^2 \right]
$$

$$
= \min_{\langle \theta_{\text{LIA}} \rangle} \left[\left(\frac{1 - \frac{T_{B_v} - T_B^\uparrow - T_B^\downarrow e^{-\tau}}{\left(T_{\text{SST}} - T_B^\downarrow \right) e^{-\tau}}}{1 - \frac{T_{B_v} - T_B^\uparrow - T_B^\downarrow e^{-\tau}}{\left(T_{\text{SST}} - T_B^\downarrow \right) e^{-\tau}}} - f\left(\langle \theta_{\text{LIA}} \rangle, \widehat{T}_{\text{SST}} \right) \right)^2 \right]
$$

$$
= \min_{\langle \theta_{\text{LIA}} \rangle} \left[\left(\frac{\left(\frac{\left(T_{\text{SST}} - T_B^\downarrow \right) e^{-\tau} - T_{B_h} + T_B^\uparrow + T_B^\downarrow e^{-\tau}}{\left(T_{\text{SST}} - T_B^\downarrow \right) e^{-\tau} - T_{B_v} + T_B^\uparrow + T_B^\downarrow e^{-\tau}} \right)}{- f\left(\langle \theta_{\text{LIA}} \rangle, \widehat{T}_{\text{SST}} \right)} \right)^2 \right]
$$

$$
= \min_{\langle \theta_{\text{LIA}} \rangle} \left[\left(\frac{T_{B_h} - T_B^\uparrow - T_{\text{SST}} e^{-\tau}}{T_{B_v} - T_B^\uparrow - T_{\text{SST}} e^{-\tau}} - f\left(\langle \theta_{\text{LIA}} \rangle, \widehat{T}_{\text{SST}} \right) \right)^2 \right].
\tag{19}
$$

If (10) and (11) are rearranged in terms of K

$$
\widehat{K} = \frac{1 - e_p}{r_p(\varepsilon, \langle \theta_{\text{LIA}} \rangle)}.
\tag{20}
$$

By substituting (15) and (16) into (18), we have for both polarizations

$$
\widehat{K} = \frac{1}{2} \sum_{p=v,h} \frac{T_{\text{SST}} e^{-\tau} - T_{B_p} + T_B^\uparrow}{r_p(\varepsilon, \langle \theta_{\text{LIA}} \rangle) \left(T_{\text{SST}} - T_B^\downarrow \right) e^{-\tau}}.
\tag{21}
$$

APPENDIX B
DURDEN AND VESECKY OCEAN WAVE HEIGHT SPECTRUM MODEL

The wave height spectrum W for a fully developed ocean proposed by Durden and Vesecky [40] (hereafter referred to as DV) is described by the following form:

$$
W(k_\rho, \phi) = \frac{1}{2\pi k_\rho} S(k_\rho) \left(1 + C_0 (1 - e^{-1.5 \times 10^{-4} k_\rho^2}) \cos 2\phi \right)
\tag{22}
$$

where $S(k_\rho)$ is the omnidirectional wave height spectrum at ocean wavenumber k_ρ, ϕ is the wave direction relative to the wind direction, and Φ is the angular spread function. $S(k_\rho)$ in (22) is modeled as

$$
S(k_\rho) = \begin{cases} a k_\rho^{-3} \exp\left(-0.74 \left(\frac{g}{k_\rho U_{19.5}^2} \right)^2 \right) & k_\rho < 2 \\ a k_\rho^{-3} \left(\frac{b k_\rho u_*^2}{g_*} \right)^{c \log\left(\frac{k_\rho}{2} \right)} & k_\rho \geq 2 \end{cases}
\tag{23}
$$

where g is the gravity acceleration constant; $U_{19.5}$ is the wind speed at 19.5 m above the sea surface; a, b, and c are the fitting coefficients; and $g_* = g + 7.25 \times 10^{-5} k_\rho$ is the modified gravity acceleration. In this study, the values of $a = 0.008$, $b = 1.75$, and $c = 0.25$ are used [40], [43].

The fitting coefficient C_0 in (22) is the ratio between crosswind to upwind slope variances for the ocean wave spectrum, which is based on the Cox and Munk [9] measured slope variances. The coefficient C_0 can be calculated as [43]

$$
C_0 = \frac{2(1 - R)}{(1 - D)(1 + R)}
\tag{24}
$$

$$
R = \frac{0.003 + 1.92 \cdot 10^{-3} U_{12.5}}{3.16 \cdot 10^{-3} U_{12.5}}
\tag{25}
$$

$$
D = \int_0^\infty k_\rho^2 S(k_\rho) \exp(-sk_\rho^2) dk_\rho \bigg/ \int_0^\infty k_\rho^2 S(k_\rho) dk_\rho
\tag{26}
$$

where $U_{12.5}$ is the wind speed at 12.5 m above the sea surface. Wind speed at arbitrary height z (U_z) above the sea surface

can be calculated from a friction velocity u_* suggested by Yueh *et al.* [43]

$$U_z = \frac{u_*}{0.4} \log_{10}\left(\frac{z}{6.84E^{-5}/u_* + 4.28E^{-3}/u_*^2 - 4.43E^{-4}}\right).$$
(27)

The mean slope variance $\langle s^2 \rangle$ of long ocean wave in an omnidirectional context can be estimated by integrating the 2-D elevation function over k_ρ and ϕ spaces, i.e.,

$$\langle s^2 \rangle = \int_0^{k_l} \int_{-\pi}^{\pi} k_\rho^2 W(k_\rho, \phi) k_\rho dk_\rho d\phi$$
(28)

where k_l is the lower cutoff wavenumber to discriminate between short and long ocean waves. In this study, $k_l = k/10$ is used [5].

In order to calculate $\langle \theta_{\text{LIA}} \rangle$, we assume that the ocean surface follows the isotropic Gaussian height distributions with the Gaussian correlation function. Therefore, a slope probability function p of the isotropic Gaussian–Gaussian surfaces can be expressed as [44]

$$p(\alpha, \beta) = \frac{1}{2\pi \sigma^2 |C''(0)|} e^{-\frac{\alpha^2 + \beta^2}{2\sigma^2 |C''(0)|}}$$
(29)

$$C(\rho) = e^{-\frac{\rho^2}{l^2}}$$
(30)

where α and β are the two orthogonal surface slope elements, $C''(\rho)$ is the second derivative of the surface height correlation function $C(\rho)$, ρ is the correlation coefficient between α and β, l is the surface correlation length, and σ^2 is the surface height variance for long ocean wave. Since $\langle s^2 \rangle$ is for tilts in α and β for the Gaussian isotropic surface, one can write $|C''(0)| = 2/l^2 = \langle s^2 \rangle/2\sigma^2$. Therefore, slope probability function can be written as

$$p(\alpha, \beta) = \frac{1}{\pi s^2} e^{-\frac{\alpha^2 + \beta^2}{s^2}}.$$
(31)

With p in (31), $\langle \theta_{\text{LIA}} \rangle$ can be calculated as

$$\langle \theta_{\text{LIA}} \rangle = \int \int_{\alpha,\beta} (\theta_{\text{EIA}} + \theta_n(\alpha, \beta)) p(\alpha, \beta) d\alpha d\beta$$
(32)

where θ_n is the angle between local and global normal vectors, which can be determined using the following relationship:

$$\theta_n(\alpha, \beta) = \cos^{-1}\left(\frac{1}{\sqrt{1 + \alpha^2 + \beta^2}}\right)$$
(33)

Equation (33) can be obtained using inner product of the normal unit vectors to global surface $\widehat{z}$ and local surface $\widehat{n}$, which are defined as [21]

$$\widehat{z} = (0, 0, 1) \quad \widehat{n} = \frac{(-\alpha, -\beta, 1)}{\sqrt{1 + \alpha^2 + \beta^2}}.$$
(34)

ACKNOWLEDGMENT

REFERENCES

[1] F. J. Wentz, "Measurement of oceanic wind vector using satellite microwave radiometers," *IEEE Trans. Geosci. Remote Sens.*, vol. 30, no. 5, pp. 960–972, Sep. 1992.

[2] T. Meissner and F. J. Wentz, "The emissivity of the ocean surface between 6 and 90 GHz over a large range of wind speeds and Earth incidence angles," *IEEE Trans. Geosci. Remote Sens.*, vol. 50, no. 8, pp. 3004–3026, Aug. 2012.

[3] A. J. Gasiewski and D. B. Kunkee, "Polarized microwave emission from water waves," *Radio Sci.*, vol. 29, no. 6, pp. 1449–1466, Nov. 1994.

[4] S. H. Yueh, W. J. Wilson, S. J. Dinardo, and F. K. Li, "Polarimetric microwave brightness signatures of ocean wind directions," *IEEE Trans. Plasma Sci.*, vol. 37, no. 2, pp. 949–959, Mar. 1999.

[5] J. T. Johnson, "An efficient two-scale model for the computation of thermal emission and atmospheric reflection from the sea surface," *IEEE Trans. Geosci. Remote Sens.*, vol. 44, no. 3, pp. 560–568, Mar. 2006.

[6] E. C. Monahan and I. G. O'Muircheartaigh, "Whitecaps and the passive remote sensing of the ocean surface," *Int. J. Remote Sens.*, vol. 7, no. 5, pp. 627–642, May 2007.

[7] D. B. Kunkee and A. J. Gasiewski, "Simulation of passive microwave wind direction signatures over the ocean using an asymmetric-wave geometrical optics model," *Radio Sci.*, vol. 32, no. 1, pp. 59–78, Jan. 1997.

[8] S. H. Yueh, "Modeling of wind direction signals in polarimetric sea surface brightness temperatures," *IEEE Trans. Geosci. Remote Sens.*, vol. 35, no. 6, pp. 1400–1418, Nov. 1997.

[9] C. Cox and W. Munk, "Measurement of the roughness of the sea surface from photographs of the sun's glitter," *J. Opt. Soc. Amer.*, vol. 44, no. 11, pp. 838–850, 1954.

[10] F. J. Wentz, "A two-scale scattering model for foam-free sea microwave brightness temperatures," *J. Geophys. Res.*, vol. 80, no. 24, pp. 3441–3446, Aug. 1975.

[11] P. A. Hwang, "Foam and roughness effects on passive microwave remote sensing of the ocean," *IEEE Trans. Geosci. Remote Sens.*, vol. 50, no. 8, pp. 2978–2985, Aug. 2012.

[12] M. H. Bettenhausen and M. D. Anguelova, "Brightness temperature sensitivity to whitecap fraction at millimeter wavelengths," *Remote Sens.*, vol. 11, no. 17, p. 2036, Aug. 2019.

[13] F. J. Wentz and T. Meissner, "Algorithm theoretical basis document (ATBD) version 2 AMSR ocean algorithm," Tech. Rep. 121599A-1, Nov. 2000, p. 66.

[14] T. Meissner and F. J. Wentz, "Wind-vector retrievals under rain with passive satellite microwave radiometers," *IEEE Trans. Geosci. Remote Sens.*, vol. 47, no. 9, pp. 3065–3083, Sep. 2009.

[15] J. Font *et al.*, "SMOS: The challenging sea surface salinity measurement from space," *Proc. IEEE*, vol. 98, no. 5, pp. 649–665, May 2010.

[16] A. Camps *et al.*, "The WISE 2000 and 2001 field experiments in support of the SMOS mission: Sea surface L-band brightness temperature observations and their application to sea surface salinity retrieval," *IEEE Trans. Geosci. Remote Sens.*, vol. 42, no. 4, pp. 804–823, Apr. 2004.

[17] S. J. English and T. J. Hewison, "Fast generic millimeter-wave emissivity model," *Proc. SPIE*, vol. 3503, pp. 288–300, Aug. 1998.

[18] N. Bormann, A. Geer, and S. English, *Evaluation of the Microwave Ocean Surface Emissivity Model in the IFS*. Reading, U.K.: ECMWF Technical Memorandum, ECMWF, Feb. 2012.

[19] Q. Liu, F. Weng, and S. J. English, "An improved fast microwave water emissivity model," *IEEE Trans. Geosci. Remote Sens.*, vol. 49, no. 4, pp. 1238–1250, Apr. 2011.

[20] S.-M. Lee and B.-J. Sohn, "A new description of small-scale and large-scale roughness in the fast ocean surface emissivity model," *J. Atmos. Ocean. Technol.*, vol. 38, no. 3, pp. 501–510, Mar. 2021.

[21] S.-M. Lee, B.-J. Sohn, and H. Shi, "Impact of ice surface and volume scatterings on the microwave sea ice apparent emissivity," *J. Geophys. Res. Atmos.*, vol. 123, pp. 9237–9920, Sep. 2018.

[22] L. Klein and C. T. Swift, "An improved model for the dielectric constant of sea water at microwave frequencies," *IEEE Trans. Antennas Propag.*, vol. AP-25, no. 1, pp. 104–111, Jan. 1977.

[23] C. Guillou *et al.*, "Impact of new permittivity measurements on sea surface emissivity modeling in microwaves," *Radio Sci.*, vol. 33, no. 3, pp. 649–667, May 1998.

[24] T. Meissner and F. J. Wentz, "The complex dielectric constant of pure and sea water from microwave satellite observations," *IEEE Trans. Geosci. Remote Sens.*, vol. 42, no. 9, pp. 1836–1849, Sep. 2004.

[25] H. J. Liebe, G. A. Hufford, and T. Manabe, "A model for the complex permittivity of water at frequencies below 1 THz," *Int. J. Infr. Millim. Waves*, vol. 12, no. 7, pp. 659–675, 1991.

[26] P. A. Stogryn *et al.*, *The Microwave Permittivity of Sea and Fresh Water*. Azusa, CA, USA: GenCorp Aerojet, 1995.

[27] K. Liou, *An Introduction to Atmospheric Radiation*, 2nd ed. San Diego, CA, USA: Academic, 2002.

[28] B. J. Sohn and S.-M. Lee, "Analytical relationship between polarized reflectivities on the specular surface," *Int. J. Remote Sens.*, vol. 34, no. 7, pp. 2368–2374, Dec. 2012.

[29] B. J. Choudhury, T. J. Schmugge, A. Chang, and R. W. Newton, "Effect of surface roughness on the microwave emission from soils," *J. Geophys. Res., Oceans*, vol. 84, no. C9, pp. 5699–5706, 1979.

[30] P. Beckmann and A. Spizzichino, *The Scattering of Electromagnetic Waves From Rough Surfaces*. Norwood, MA, USA: Artech House, 1987.

[31] L. Tsang, J. A. Kong, and R. T. Shin, *Theory of Microwave Remote Sensing*, vol. 613. Hoboken, NJ, USA: Wiley, 1985.

[32] R. T. Tonboe, G. DybkjÆR, and J. L. HøYer, "Simulations of the snow covered sea ice surface temperature and microwave effective temperature," *Tellus A, Dyn. Meteorol. Oceanogr.*, vol. 63, no. 5, pp. 1028–1037, Jan. 2011.

[33] S.-M. Lee, B.-J. Sohn, and C. Kummerow, "Long-term Arctic snow/ice interface temperature from special sensor for microwave imager measurements," *Remote Sens.*, vol. 10, no. 11, p. 1795, Nov. 2018.

[34] H. Masunaga *et al.*, "Satellite data simulator unit: A multisensor, multispectral satellite simulator package," *Bull. Amer. Meteorol. Soc.*, vol. 91, no. 12, pp. 1625–1632, 2010.

[35] D. P. Dee *et al.*, "The ERA-interim reanalysis: Configuration and performance of the data assimilation system," *Q. J. Roy. Meteorol. Soc.*, vol. 136, pp. 553–597, Apr. 2011.

[36] M. Zweng *et al.*, "World ocean atlas 2013, salinity," NOAA Atlas NESDIS, Silver Spring, MD, USA, Tech. Rep. 74, 2013, vol. 2.

[37] T. Elfouhaily, B. Chapron, K. Katsaros, and D. Vandemark, "A unified directional spectrum for long and short wind-driven waves," *J. Geophys. Res.*, vol. 102, no. C7, pp. 15781–15796, 1997.

[38] K. Hasselmann *et al.*, "Measurements of wind-wave growth and swell during the joint north sea wave project (JONSWAP)," *Ergaenzungsheft Zur Deutschen Hydrographischen Zeitschrift, Reihe A*, vol. 8, no. 12, pp. 1–95, Jan. 1973.

[39] M. A. Donelan, J. Hamilton, and W. H. Hui, "Directional spectra of wind generated waves," *Philos. Trans. R. Soc. London, Ser. A.*, vol. 315, no. 1534, pp. 509–562, Sep. 1985.

[40] S. Durden and J. Vesecky, "A physical radar cross-section model for a wind-driven sea with swell," *IEEE J. Ocean. Eng.*, vol. OE-10, no. 4, pp. 445–451, Oct. 1985.

[41] A. Stogryn, "The emissivity of sea foam at microwave frequencies," *J. Geophys. Res.*, vol. 77, no. 9, pp. 1658–1666, Mar. 1972.

[42] W. J. Pierson and L. Moskowitz, "A proposed spectral form for fully developed wind sea based on the similarity theory of S. A. Kitaigorodskii," *J. Geoyphs. Res.*, vol. 69, no. 24, pp. 5181–5190, Dec. 1964.

[43] S. H. Yueh, R. Kwok, F. K. Li, S. V. Nghiem, W. J. Wilson, and J. A. Kong, "Polarimetric passive remote sensing of ocean wind vectors," *Radio Sci.*, vol. 29, no. 4, pp. 799–814, Jul. 1994.

[44] A. J. Gasiewski, "Class lecture, topic: 'Electromagnetic absorption, scattering, and propagation'," Elect., Comput., Energy Eng., Univ. Colorado, Boulder, Boulder, CO, USA, Tech. Rep. ECEN5264, Apr. 2021.

[45] J. T. Johnson and M. Zhang, "Theoretical study of the small slope approximation for ocean polarimetric thermal emission," *IEEE Trans. Geosci. Remote Sens.*, vol. 37, no. 5, pp. 2305–2316, Sep. 1999.

[46] V. G. Irisov, "Small-slope expansion for thermal and reflected radiation from a rough surface," *Waves Random Media*, vol. 7, no. 1, pp. 1–10, Jan. 1997.

[47] M. Kazumori and S. J. English, "Use of the ocean surface wind direction signal in microwave radiance assimilation," *Quart. J. Roy. Meteorolog. Soc.*, vol. 141, no. 689, pp. 1354–1375, Apr. 2015.

[48] T. Meissner and F. Wentz, "An updated analysis of the ocean surface wind direction signal in passive microwave brightness temperatures," *IEEE Trans. Geosci. Remote Sens.*, vol. 40, no. 6, pp. 1230–1240, Jun. 2002.

[49] D. H. Staelin, "Measurements and interpretation of the microwave spectrum of the terrestrial atmosphere near 1-centimeter wavelength," *J. Geophys. Res.*, vol. 71, no. 12, pp. 2875–2881, Jun. 1966.

[50] F. T., Ulaby, R. K. Moore, and A. K. Fung, *Microwave remote sensing: Active and Passive, Microwave Remote Sensing Fundamentals and Radiometry*, vol. 1. Reading, MA, USA: Addison-Wesley, 1981, p. 456.

[51] M. Kasahara *et al.*, "Status of AMSR2 on GCOM-W1," *Proc. SPIE*, vol. 8533, Nov. 2012, Art. no. 853307.

[52] T. Kimura, "Overview of Japanese Earth observation programs," *Proc. SPIE*, vol. 11530, Sep. 2020, Art. no. 74740G.

[53] N. Ebuchi, "Evaluation of Marine surface wind speed observed by AMSR2 on GCOM-W," *IEEE J. Sel. Topics Appl. Earth Observ. Remote Sens.*, vol. 10, no. 9, pp. 3955–3962, Sep. 2017.

Sang-Moo Lee (Member, IEEE) was born in Seoul, Republic of Korea, in 1989. He received the B.S. and Ph.D. degrees in earth environmental science from Seoul National University, Seoul, Republic of Korea, in 2011 and 2018, respectively.

From 2018 to 2019, he was a Post-Doctoral Research Scientist with the Satellite Meteorology Laboratory, Seoul National University. In 2019, he was an Research Assistant Professor with Brain Korea 21 plus project of Seoul National University. He is currently a Post-Doctoral Research Fellow with the Department of Electrical, Computer, and Energy Engineering, University of Colorado Boulder, Boulder, CO, USA, and a Visiting Scholar with the National Snow and Ice Data Center, Cooperative Institute for Research in Environmental Sciences, University of Colorado Boulder. His research interests include satellite remote sensing, the utilization of satellite measurements to study oceanic and atmospheric processes, and the modeling of the radiative transfer and surface emissivity.

Albin J. Gasiewski (Fellow, IEEE) received the B.S. and M.S. degrees in electrical engineering and the B.S. degree in mathematics from Case Western Reserve University, Cleveland, OH, USA, in 1983, and the Ph.D. degree in electrical engineering and computer science from the Massachusetts Institute of Technology, Cambridge, MA, USA, in 1989.

From 1989 to 1997, he was a Faculty Member with the Georgia Institute of Technology, Atlanta, GA, USA. From 1997 to 2005, he worked with U.S. National Oceanic and Atmospheric Administration's (NOAA) Environmental Technology Laboratory, Boulder, CO, USA, where he became the Chief of the ETL's Microwave Systems Development Division. He has developed and taught graduate courses on electromagnetics, antennas, remote sensing, instrumentation, and wave propagation theory. He is a Co-Founder and the Chief Scientist of Orbital Micro Systems, Inc., Boulder. He is currently a Professor of electrical and computer engineering with the University of Colorado Boulder, Boulder, and the Director of the CU Center for Environmental Technology (CET).

Dr. Gasiewski was the Past President from 2004 to 2005 of the IEEE Geoscience and Remote Sensing Society (IGARSS), the Founding Member of the IEEE Committee on Earth Observation (ICEO), and also a member of the American Meteorological Society, the American Geophysical Union, the International Union of Radio Scientists (URSI), Tau Beta Pi, and Sigma Xi. He was a recipient of the 2006 Outstanding Service Award and the 2017 Education Award from the GRSS. From 2009 to 2011, he served as the Chair for the U.S. National Committee (USNC)/URSI Commission F. He served for the U.S. National Research Council's Committee on Radio Frequencies (CORF) from 1989 to 1995. He was the General Co-Chair of IGARSS 2006, Denver, CO.

Byung-Ju Sohn received the B.S. degree in earth science and the M.S. degree in meteorology from Seoul National University, Seoul, Republic of Korea, in 1980 and 1985, respectively, and the Ph.D. degree in meteorology from Florida State University, Tallahassee, FL, USA, in 1990.

After the postdoctoral work at the NASA Marshall Space Flight Center in Huntsville, AL, USA, he joined Seoul National University as a Faculty Member in 1993. He has been focusing on the satellite meteorology studying radiation physics and satellite remote sensing, for better understanding and interpreting the weather and climate phenomena from satellite measurements. He has served various administration positions and professional services including the Head of School of Earth and Environmental Sciences of Seoul National University, the President of the Korean Meteorological Society (2016–2017), and the WCRP GEWEX Science Steering Group Member. He was the President of International Radiation Commission (2017–2020) associated with IUGG/IAMAS and a member of Korea Academy of Science and Technology. He is also an Honorary Professor of NUIST in Nanjing, China.